**Author(s):** Romppanen, Sari; Häkkänen, Heikki; Kaski, Saara

**Title:** Singular value decomposition approach to the yttrium occurrence in mineral maps of rare earth element ores using laser-induced breakdown spectroscopy

**Year:** 2017

**Version:**

**Please cite the original version:**

Romppanen, S., Häkkänen, H., & Kaski, S. (2017). Singular value decomposition approach to the yttrium occurrence in mineral maps of rare earth element ores using laser-induced breakdown spectroscopy. Spectrochimica Acta Part B: Atomic Spectroscopy, 134, 69-74. https://doi.org/10.1016/j.sab.2017.06.002

# Accepted Manuscript


Singular value decomposition approach to the yttrium occurrence in mineral maps of rare earth element ores using laser-induced breakdown spectroscopy

Sari Romppanen, Heikki Häkkänen, Saara Kaski

PII: S0584-8547(17)30132-5
DOI: doi: 10.1016/j.sab.2017.06.002
Reference: SAB 5258

To appear in: *Spectrochimica Acta Part B: Atomic Spectroscopy*

Received date: 28 February 2017
Revised date: 15 May 2017
Accepted date: 3 June 2017

Please cite this article as: Sari Romppanen, Heikki Häkkänen, Saara Kaski , Singular value decomposition approach to the yttrium occurrence in mineral maps of rare earth element ores using laser-induced breakdown spectroscopy, *Spectrochimica Acta Part B: Atomic Spectroscopy* (2017), doi: 10.1016/j.sab.2017.06.002

# Singular value decomposition approach to the yttrium occurrence in mineral maps of rare earth element ores using laser-induced breakdown spectroscopy

**Sari Romppanen[a], Heikki Häkkänen[b] and Saara Kaski[a]**

*[a]Department of Chemistry, P.O.BOX 35 FI-40014 University of Jyväskylä, Finland*
*[b]Dept. of Biological and Environmental Science, P.O.BOX 35 FI-40014 University of Jyväskylä, Finland*
*Corresponding author E-mail address: saara.kaski@jyu.fi (S.Kaski)*

## Abstract

Laser-induced breakdown spectroscopy (LIBS) has been used in analysis of rare earth element (REE) ores from the geological formation of Norra Kärr Alkaline Complex in southern Sweden. Yttrium has been detected in eudialyte ($Na_{15}$ $Ca_6(Fe,Mn)_3$ $Zr_3Si(Si_{25}O_{73})(O,OH,H_2O)_3$ $(OH,Cl)_2$) and catapleiite ($Ca/Na_2ZrSi_3O_9 \cdot 2H_2O$). Singular value decomposition (SVD) has been employed in classification of the minerals in the rock samples and maps representing the mineralogy in the sampled area have been constructed. Based on the SVD classification the percentage of the yttrium-bearing ore minerals can be calculated even in fine-grained rock samples.

**Keywords:** Yttrium, Laser-Induced Breakdown Spectroscopy (LIBS), Singular value decomposition, Mineral mapping, Rock analysis

## 1. Introduction

Yttrium belongs to the group of rare earth metals, REMs (also known as rare earth elements; REEs) with scandium and lanthanoids [1]. European commission has classified rare earth elements as critical material for EU due to high supply risk as well as economic importance [2]. Recently the EU Commission has divided REEs in to two groups, heavy rare earth elements (HREEs) and light rare earth elements (LREEs) and scandium. Yttrium belongs to HREEs and their demand has been predicted to increase in the future, which could lead to possible deficit in 2020. The importance on REEs for modern technology is caused by their specific optical, electrical and magnetic properties [3]. Yttrium is mainly used as raw material in ceramics, metallurgy, and phosphors. A well-known example is a yttrium-aluminum-garnet crystal used in Nd:YAG lasers. In many of these applications, yttrium is hard to substitute with another material without losing the functionality. In year 2016 yttrium oxide was consumed 3000 to 6000 tons globally, mostly to form very pure oxide compounds for luminescent phosphors. Word production of yttrium was estimated to be 5000–7000 tons. Currently yttrium, along with other REEs, is mainly supplied in China [4]. Worldwide resources are supposed to be large, because yttrium occurs in most of the REE deposits [5,6]. In geological environments, yttrium can be found in many different minerals in various concentrations.

In this research, laser-induced breakdown spectroscopy (LIBS) has been utilized to mapping of yttrium-bearing rocks. For mining purposes, ore bodies are 3D-modelled based on different geological measurements and various analyzed samples. We have constructed mineral maps, which offer fast and informative description of the mineralogical and elemental distribution of the drill core samples. Many tasks in mining processes as well as in mill processes could also gain profit of this kind of specification of rocks. For example, the texture i.e. the grain size and the shape of the minerals and the location of the gangue minerals can complicate the beneficiation of the ore.

The applications of LIBS in analysis of various geological materials have been reviewed in detail by Harmon et al. [7] and the strongest evidence of the capability of LIBS is the still continuous operation of the ChemCam analyzer in planetary exploration in Mars [8]. The first reported LIBS research on yttrium by Ishizuka [9] thoroughly studied the plasma dimensions, emission intensities and the calibration curves of several REEs in different salt matrices. As a result, lowest limit of detection for yttrium was 2 ppm and it was observed in sodium chloride matrix. Harilal et al. [10] used LIBS on yttrium to analyze temporal and spatial changes in a laser-induced plasma generated on a superconductor $YBa_2Cu_3O_7$ and Buckley et al. [11] detected yttrium in the exhaust fumes. Yttrium solutions, among others, have been used to compare LIBS and inductively coupled plasma spectroscopy (ICP-OES) by Fichet et al. [12] and a detection limit of 0.8 mg/L was obtained. Extensive list of emission lines based on the REE samples prepared from reference materials at mass percentages of 1 to 50 has been provided by Martin et al. [13]. Just recently, Labutin et al. [14] have been able to determine limit of detection for yttrium, 0.6 ppm, using certified geological reference materials and plasma modeling.

Instead of quantitative analysis of yttrium, the aim of this research was identification of the yttrium-bearing minerals using singular value decomposition (SVD). It offers a possibility to

find structure between the observations and the data variables, which can be used to extract the most important information to represent the data.

## 2. Experimental

*2.1 Samples*

The three diamond drill core samples from Norra Kärr deposit were selected for the LIBS analysis. The geological formation of Norra Kärr Alkaline Complex in southern Sweden consists on agpaitic nepheline syenites, also called as grennaite, which is a rock type rich in zirconium and rare-earth elements. The samples consist of typical PGT grennaite (grennaite with pegmatite), in which fine-grained greenish aegirine-rich ground mass contains leucosomic coarser pegmatitic sections, where mineral composition is nepheline altered to zeolite (natrolite–analcime), microcline, albite, eudialyte and catapleiite [15,16]. This PGT-type of mineralization covers about 75 % of Norra Kärr's mineral resource. The main minerals of these PGT-rocks and examples of their chemical formulas are presented in Table 1. In minerals, the ratio of the cations may vary and partly they may have been substituted by other similar-sized elements even inside a single crystal. Thus, the chemical formulas given are in general form. The potential ore minerals of Norra Kärr are eudialyte and catapleiite, whereas the aegirine, all the feldspars and the feldspathoid nepheline are unworthy gangue minerals.

**Table 1.** Main minerals of PGT-type grennaite in Norra Kärr deposit.

| Mineral | Typical chemical formula | *wt%*[15] |
|---|---|---|
| Aegirine | $NaFeSi_2O_6$ | 21.4 |
| Nepheline | $(Na,K)AlSiO_4$ | 11.2 |
| Natrolite - Analcime | $Na_2Al_2Si_3O_{10} \cdot 2H_2O$ - $NaAlSi_2O_6 \cdot H_2O$ | 16.3 |
| Microcline | $KAlSi_3O_8$ | 16.0 |
| Albite | $NaAlSi_3O_8$ | 17.7 |
| Anorthoclase | $(Na,K)AlSi_3O_8$ | 1.3 |
| Eudialyte | $Na_{15}Ca_6(Fe,Mn)_3Zr_3Si(Si_{25}O_{73})(O,OH,H_2O)_3(OH,Cl)_2$ | 8.2 |
| Catapleiite | $Ca/Na_2ZrSi_3O_9 \cdot 2H_2O$ | 4.0 |

In general, REE grades in eudialyte may be lower than those of other REE-minerals monazite and xenotime, but in eudialyte, the HREE content is high and the environmentally hazardous uranium and thorium contents are lower [5]. Especially in Norra Kärr deposit the proportion of the valuable HREEs, including yttrium, is high. It has been investigated, that the eudialyte minerals contain as high as 95 % of REEs of Norra Kärr. Also, economically interesting zirconosilicate mineral, catapleiite, occurs in the deposit. The total REE and zirconium contents as oxides in specific coarse-grained PGT have been analyzed at concentrations of 0.62 % and 2.01 %, respectively [15]. On average the yttrium content in Norra Kärr eudialyte is 1.3 % [17]. This indicates, that some cations of eudialyte have been substituted by yttrium and due to the chemical similarity, by other HREEs.

*2.2. Setup*

Plasma was generated by focusing a KrF excimer laser (Optex, Lambda Physik) into the surface of a sample at spot size of 200 µm in diameter. Average pulse energy of ~2.5 mJ corresponds to irradiance of approximately 0.9 GW/cm$^2$. The plasma emission was collected via fused silica fiber. Fiber head was fixed to 30º angle from the laser beam and the distance

from the plasma plume was 1 cm. Plasma light was dispersed in a 150 mm Czerny-Turner type imaging spectrograph (Acton, SP-150), resolution was 0.2 nm.

An intensified charge coupled device (ICCD) with a 1024 x 256 pixel imaging area and an 18-mm intensifier (InstaSpec V, Oriel) was used in recording the spectra. The delay time of 1 µs and the gate width of 2 µs were found optimal for these measurements and were controlled by a delay generator (model DG 535, Stanford Research System, Inc.). From all three samples a 1.5 cm x 1.5 cm area was measured resulting in with 60 x 60 spectra. At each location 5 laser shots were accumulated to produce a LIBS spectrum.

*2.3. Data processing*

The spectral data was decomposed with SVD using MATLAB R2015a software (The MathWorks, Inc.) from the original raw data (except for the background correction in the detector). The spectra were arranged to a matrix containing 60 x 180 measurements and each consisted of 701 pixels, which corresponded to the image intensified area of the 1024 pixel detector representing the spectral region of 389 nm – 417 nm.

## 3. Results and discussions

The mathematical formulation in detail of the singular value decomposition can be found elsewhere [18–20], but the schematic diagram in Fig. 1 demonstrates the variables in this research given by SVD function [21]. U and V are orthogonal normalized matrices and the columns of U and V are called left and right singular vectors, respectively. S is a diagonal matrix containing the singular values, which are positive and sorted in the decreasing order.

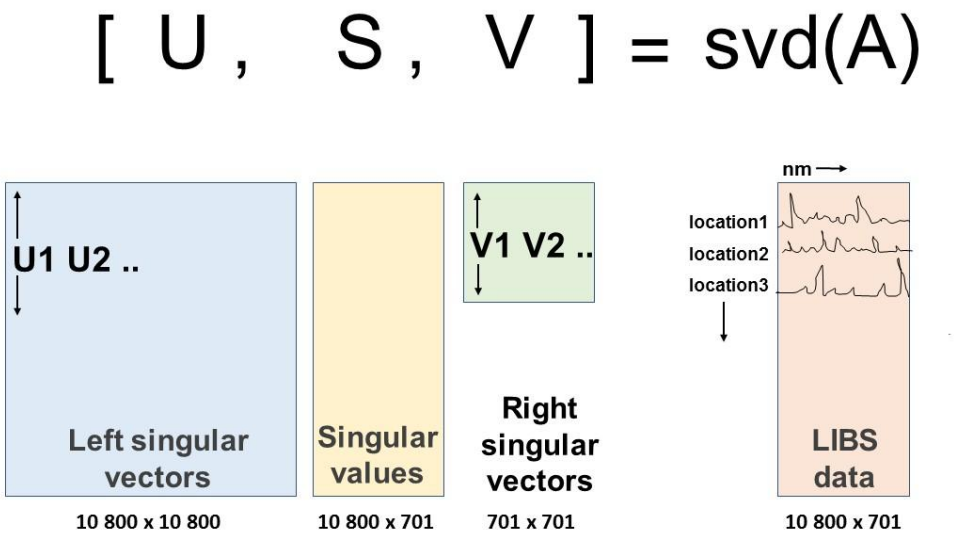


**Fig. 1.** Schematic diagram of the outcome of the singular value decomposition on the analyzed LIBS data.

SVD is related to the principal component analysis (PCA). If the spectral data in A is centered column wise as it typically is in PCA, the results are equal: right singular vectors given as columns of the matrix V correspond to the principal components, also known as loadings, and the matrix U*S contains the scores of PCA [20]. The feasibility of PCA on LIBS spectra in constructing of high-resolution maps has been recently demonstrated by Klus

et al. [22], which based on the idea that the first principal component represents the variation caused solely by the uranium and its score values show the location of the ore.

In our approach the matrices obtained via SVD are used directly for the classification of the spectral data. Firstly, the spectral data matrix has not been pre-processed. The discussion of the influence of the LIBS data treatment, including data centering, to the multivariate data analysis can be found in detail elsewhere [23], but in this case the raw data is optimal to find the differences in several minerals. When the data is not centered, the first component spectrum typically represents approximate average spectrum and the others show changes respective to it [24]. The SVD components V1 – V4, which explain 99.5 percent of the variance of the LIBS data (calculated from $S^2$), are presented in Fig. 2. If the value of V is close to zero at certain wavelenght it has only a little contribution to the component. A high positive or negative load, on the other hand, suggests a strong contribution of the wavelength to the component in question [25]. Some selected waveleghts of representative elements describing the sample minerals have been marked to the spectrum in Fig. 2 to guide the eye. As the analysis is based on the whole spectrum in the range of 389 nm – 417 nm, the laborious identification of spectral lines with dense, overlapping spectra of zirconium, iron and yttrium is not needed. With strong negative peaks, V1 correlates to the existence of aluminum and calcium. V2 has a strong positive peak of calcium and also smaller peaks for yttrium and iron, where as the aluminum peak is negative. V3 correlates to silicon and iron on positive peaks and to yttrium on negative peaks. V4 shows positive peaks of iron and yttrium, where as others are negligible.

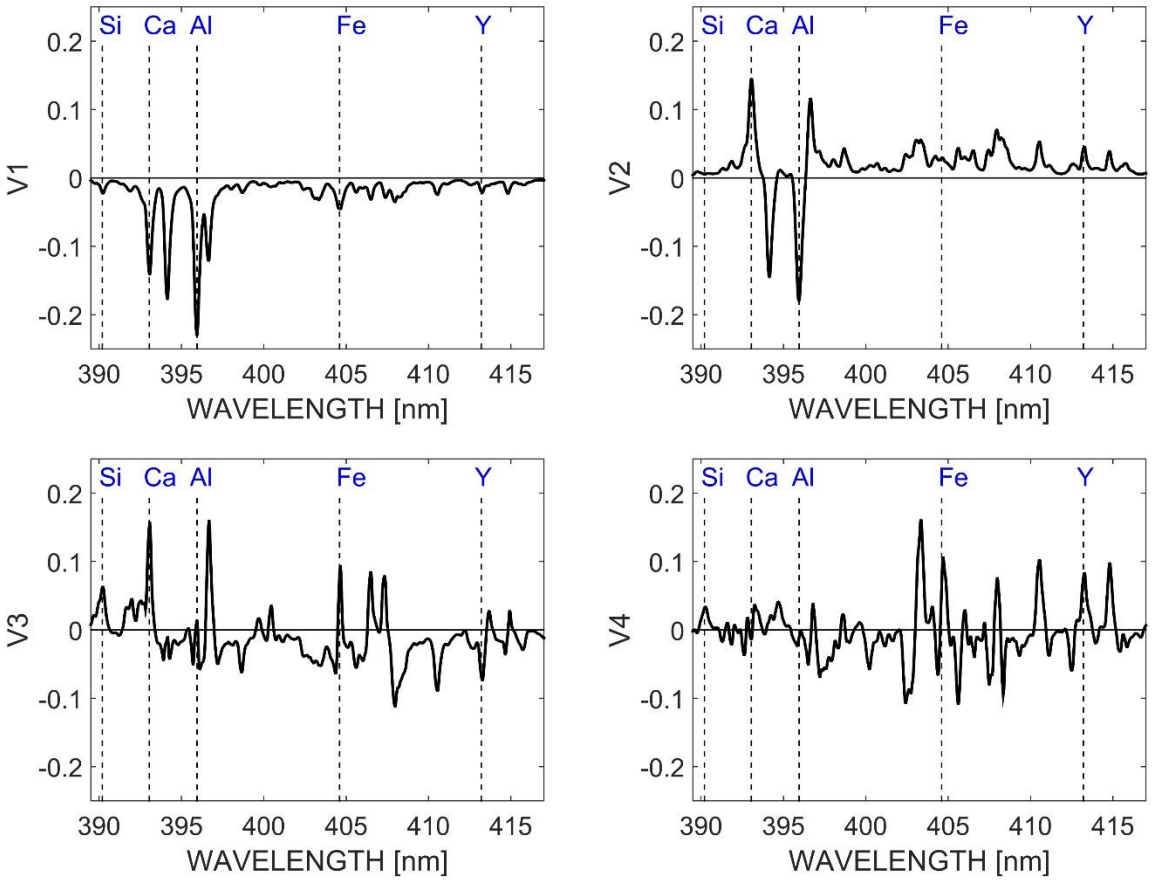

**Fig. 2.** Right singular vectors V1 – V4 calculated by SVD from the LIBS spectra measured from Norra Kärr drill core samples. Lines of the silicon, calcium, aluminum, iron and yttrium are presented in x-axis to show the contribution of selected elements to the components.

The matrix U works as a scaled version of the PCA scores [18] and the maps in Fig. 3 show values of the U in each measurement point with respect to the first four SVD components. The values of U1 regarding to the first component V1 were all negative, but other three show both positive and negative values. Sign of the U value (Fig. 3) controls the appearance of the certain peaks in component spectra (Fig. 2) and the magnitude has an impact to the intensity.

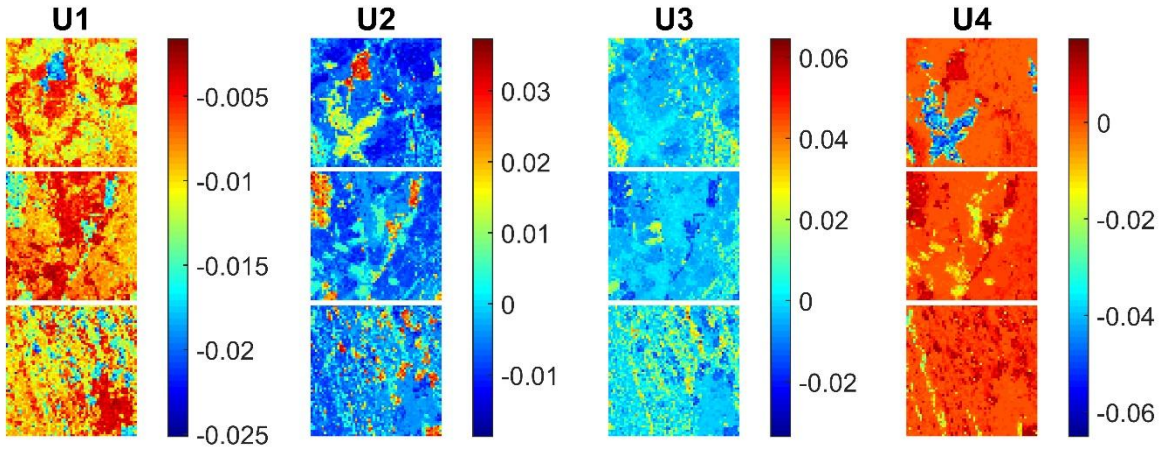


**Fig. 3.** Left singular vectors U1 – U4 for each measured location are presented as colored maps for three Norra Kärr samples. Note the different numerical scale on each plot.

The mineral composition of sample was classified according to sign of the singular vectors U2, U3 and U4. It was assumed, that the similar shaped spectra would tend to cluster in a particular region according to their geochemical composition. As the values of U1 were all negative and the corresponding component V1 had a form of negative average spectrum, it was excluded from this analysis. The values of U2, U3 and U4 were divided to 8 different regions described by the octant notation. For example, when the values were all positive, the octant region was marked as "+++" and as "---" when all three were negative.

All data points were classified to one of these octants and were presented in colors to provide maps of the samples, named A, B and C, in Fig. 4 (1). As a reference, the photo, where the main minerals have been macroscopically identified in Fig. 4 (2) is shown. It can be observed, that the map based on SVD classification follows the locations of the coarser grained areas. In photo taken under UV laser light (Fig. 4 (3)) catapleiite can be recognized due to the strong green luminescence, which is typical to the Norra Kärr catapleiite and is caused by uranyl ion $(UO_2)^{2+}$. Other luminescence colors may also correlate to certain minerals, as luminescence often is an indication of presence of an activator element in the mineral structure [26]. In addition, the yttrium distribution determined as intensity from yttrium line at 412.8 nm [27] is presented in Fig. 4 (4).

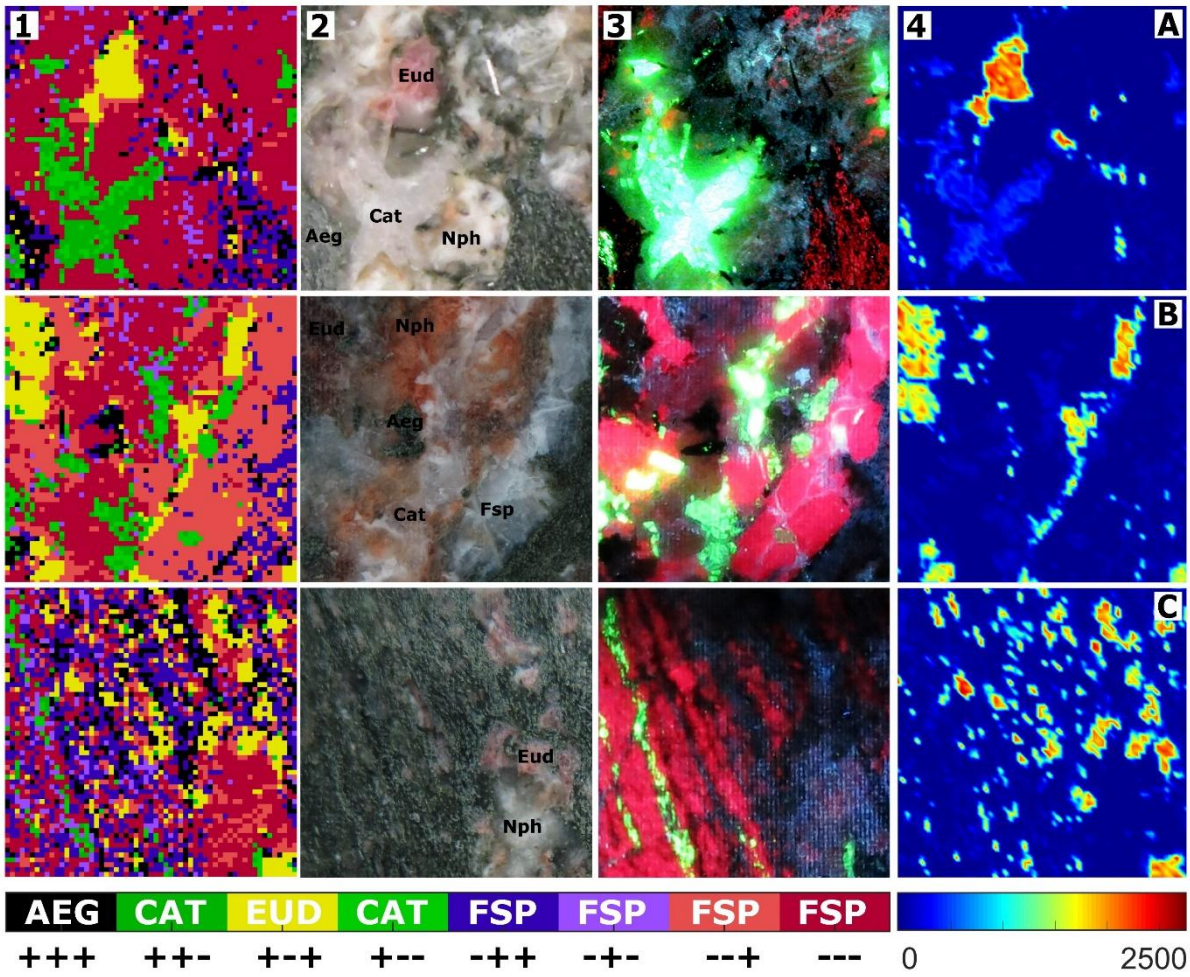


**Fig. 4. (**1) Mineral classification, based on the singular value decomposition using left singular vectors U2, U3 and U4, was carried out simultaneously for three Norra Kärr samples (A, B, C). Each color represents one octant, e.g. yellow areas correspond to the data points, where the values of U2 and U4 were positive and U3 negative (+-+). The results are compared to the (2) photo of the measured area. Mineral abbreviation Eud stands for eudialyte, Aeg for aegerine, Cat for catapleiite, Nph for nepheline and Fsp for feldspar minerals. In (3) corresponding luminescence photo under UV laser light (248 nm) is presented and in 4) distribution of yttrium emission intensity at 412.8 nm, where darkest blue corresponds negligible values.

Based on the classification results, the original data was used to generate average spectra of all the measured locations belonging to specific color. The eight spectra are presented in Fig. 5, and final division to corresponding mineral types has been based on the strongest spectral features in them. Again, only some emission lines are marked to the spectrum to support the analysis.

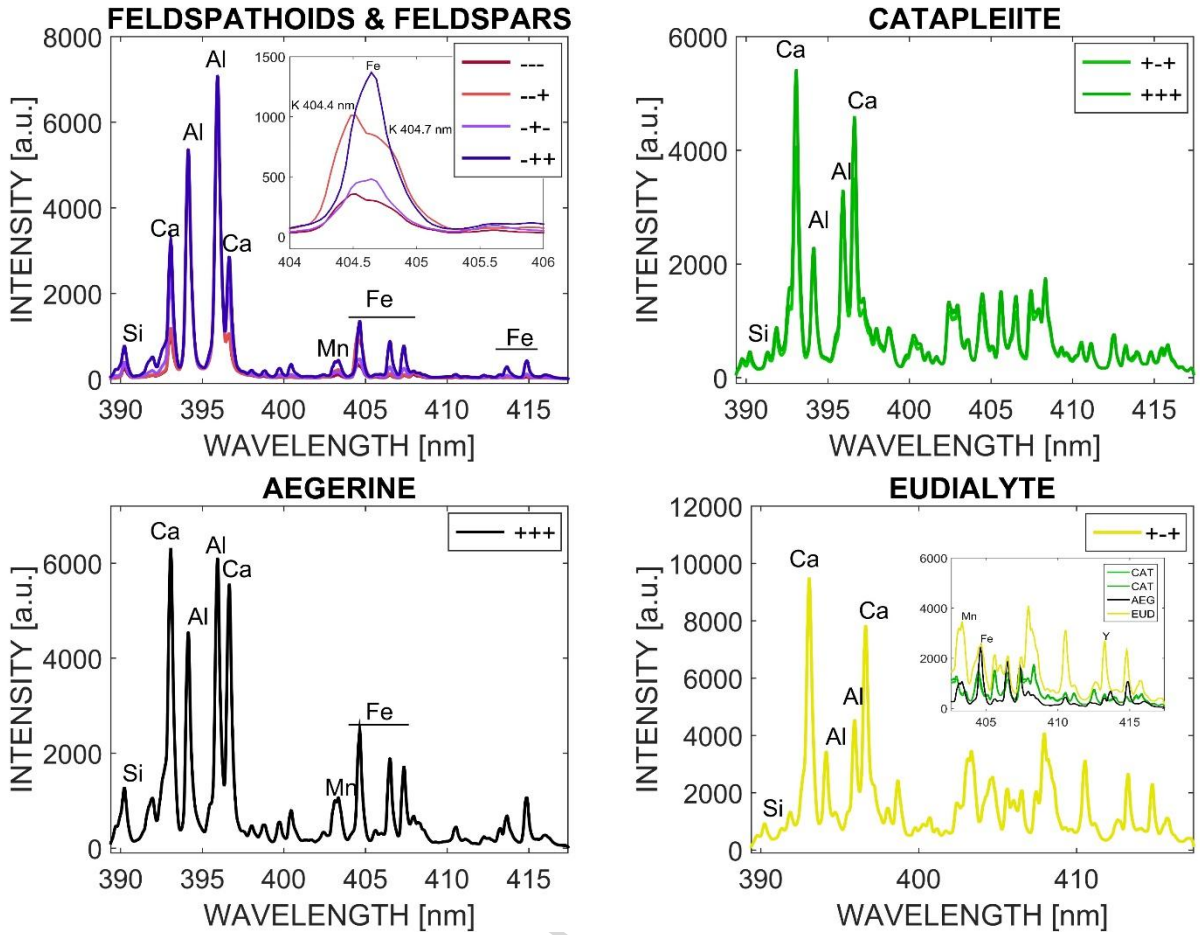


**Fig. 5.** Each color spectrum represent the average, which has been calculated from the original spectral data belonging to specific color shown in Fig. 4. Similar spectra are illustrated in the same subplot to demonstrate the respective resemblance. Small insert spectra show the differences in the spectral features of feldspar/feldspathoid minerals (up left) and eudialyte, catapleiites and aegerine (down right).

The areas in the map under dark red, light red, blue and violet have been recognized as feldspar and feldspathoid minerals. Spectral lines of potassium can be seen as side wings in the both red spectra (insert in Fig. 5). The average contents (*wt-%*) of potassium in Norra Kärr microcline and nepheline are 8.99 % and 2.32 %, respectively [28], so the light red areas in Fig. 4 (4) most likely are microcline and dark red are feldspathoid nepheline. The black colored group belong to the aegirine, since iron and silicon contents are high in the average spectrum. The two green average spectra differ only slightly on their relative intensities, mostly of calcium. The respective locations in the map have been recognized in the areas, where the catapleiite mineral emits strong green luminescence in Fig. 4 (3). The yellow areas correlate to the locations of reddish eudialyte mineral in the photos in Fig. 4 (2). The intensities of yttrium, iron and manganese lines are strong in yellow spectrum and the lines are wide due to the occurrence of the zirconium, although not marked to the spectra. The comparison of green spectra of catapleiite to the other zirconium-rich mineral eudialyte and to the iron-rich aegirine is shown in another insert in Fig. 5. The green catapleiite spectra do not contain lines of manganese or iron, but otherwise follows the spectral lines of the yellow eudialyte, which is congruent to the mineral compositions in Table 1.

The correlation between the mineral locations and the areas classified by the SVD was very good as shown in Fig. 4. As a result, the content of the ore minerals eudialyte and catapleiite

could be determined for the analyzed samples (Table 2). In the fine-grained areas of sample C, the macroscopic identification of minerals is very challenging, even impossible. The estimated percentage level of eudialyte (12 % of the measured points) most likely would not have been obtained without the SVD classification based on the LIBS analysis. For these kinds of samples the complementary laser spectroscopic method Raman, which in general is very powerful in mineral identification, suffers from the strong fluorescent background.

**Table 2.** Mineral percentages in three sampled areas based on the SVD classification of the LIBS spectra.

| % | A | B | C |
|---|---|---|---|
| Eudialyte | 4 | 12 | 12 |
| Catapleiite | 12 | 10 | 4 |
| Gangue minerals | 83 | 78 | 84 |

SVD classification could be carried out to any LIBS spectra measured, but the spectral range, which optimally describes the changes in the minerals of interest, must be selected with care. When aiming to the potential use in on-line sorting, the use of high resolution spectrum at wide spectral range quickly increases the data handling time and thus it is necessary to find a compromise. In this research, the spectra measured from 389 nm – 417 nm was optimally describing the Norra Kärr PGT samples. If more lines would have been included to the study, their contribution might have been dominating the first components and the separation would have needed more values of singular vectors U. On the other hand, without certain lines, the identification is more approximate. This was observed, when sorting was also tried separately for sample A in the spectral regions of 401 nm – 428 nm and 283 nm – 317 nm. In general, the first case lacks lines of silicon and aluminum, but shows yttrium, zirconium, iron and calcium. An oversimplified conclusion of this test was that map generated at this range describes best the eudialyte and catapleiite minerals and the gangue minerals are not separated well enough. The latter spectral range shows strong lines of silicon, aluminum, and calcium and, respectively, classifies better the gangue minerals but does not see difference between catapleiite and eudialyte. By combining these spectral ranges similar classification to the one given in Fig 4. can be obtained, which can be seen as a proof of the optimal performance obtained by spectra measured at 389 nm – 417 nm.

This classification describes only the major differences in the spectra, because the number of vectors is limited. If there are only few points in the data set for specific mineral of interest, it may not be included to the selected components. To demonstrate this, the classification was carried out also separately on each sample A, B and C at the optimal spectral range between 389 nm and 417 nm. As a result, the catapleiite mineral was not found from the sample C. When the average spectra obtained from sample C were taken under study, it was realized, that method rather found differences in the intensities of the main emission lines in the larger groups of data points instead of detecting the change in the relatively weaker yttrium lines of catapleiite. The percentage catapleiite in the sample C was only 4, corresponding to 144 measurement points. On the contrary, although the eudialyte content in sample A was same 4 %, it was clearly seen at the sampled locations. This can be explained by the greater difference in the spectrum, as eudialyte has strong lines of yttrium, zirconium, and manganese in the range 404 nm (Fig. 5).

The appearance of calcium and aluminum in Fig 5. despite the general chemical formula given in Table 1 can be either seen as an indicator of an occurrence of many minerals at the measured location or the occurred replacement of cations in the minerals. At the borders of mineral grains, the laser most likely hits simultaneously to two or even more different minerals and thus the obtained spectrum is a mixture of these. Also the chemical variations in minerals are common and the analysis based on SVD is not meant to be that exact to differentiate all of those. Thus, the average spectra may be somewhat misleading for the recognition of the minerals. Especially for the elements with weak intensities, it could be useful to check how much spectrum in measured location differs from an average one. For example, yttrium lines could be observed, in descending order of intensity, in the average spectra of eudialyte (yellow), catapleiite (greens) and aegirine (black) in Fig. 5. The map constructed of the intensity distribution of yttrium line in Fig. 4 (4) reveals, that yttrium rarely occurs at the regions of aegirine in these samples.

## 4. Conclusions

An approach based on SVD on the LIBS spectra can be used extract the mineralogical information of rock samples. The classification of all spectral points based on the singular vectors can be used to construct a map representing the mineralogy and geological texture at the sampled area. The minerals can be identified based on the average spectra from the original data. There may be a possibility to detect also the chemical alterations of minerals, but care must be taken in the interpretation of the results and the use of the original data in addition to the average spectra is recommended. A prior knowledge of the minerals to be identified is a benefit in the selection of a representative spectral range, but the method can be used as a first approach to discriminate and visualize any spectral data.

## Acknowledgements

This research is supported by the Academy of Finland (Grant 281955 to S.K. and Grant 282240 to H.H.). The Norra Kärr samples were kindly provided by Tasman Metals AB (currently Leading Edge Materials).

## References

[1] N.G. Connelly, Nomenclature of inorganic chemistry: IUPAC recommendations 2005. The red book., Royal Society of Chemistry, Cambridge, 2005.

[2] E. Commission, Critical Raw Materials for the EU. Report of the Ad-hoc Working Group on Defining Critical Raw Materials, (2010) 53.

[3] European Commission, Report on critical raw materials for the EU, Report of the Ad hoc Working Group on defining critical raw materials, (2014) 41. http://ec.europa.eu/enterprise/policies/raw-materials/files/docs/crm-report-on-critical-raw-materials_en.pdf.

[4] U.S. Geological Survey, Mineral Commodity Summaries, 2017. doi:https://doi.org/10.3133/70180197.

[5] K.M. Goodenough, J. Schilling, E. Jonsson, P. Kalvig, N. Charles, J. Tuduri, E.A. Deady, M. Sadeghi, H. Schiellerup, A. Müller, G. Bertrand, N. Arvanitidis, D.G. Eliopoulos, R.A. Shaw, K. Thrane, N. Keulen, Europes rare earth element resource potential : An overview of REE metallogenetic provinces and their geodynamic setting, Ore Geol. Rev. 72 (2016) 838–856. doi:10.1016/j.oregeorev.2015.09.019.

[6] K.R. Long, B.S. Van Gosen, N.K. Foley, D. Cordier, The Principal Rare Earth Elements Deposits of the United States — A Summary of Domestic Deposits and a Global Perspective, US Geol. Surv. Sci. Investig. 89 (2010) 8. doi:10.1007/978-90-481-8679-2_7.

[7] R.S. Harmon, R.E. Russo, R.R. Hark, Applications of laser-induced breakdown spectroscopy for geochemical and environmental analysis: A comprehensive review, Spectrochim. Acta - Part B At. Spectrosc. 87 (2013) 11–26. doi:10.1016/j.sab.2013.05.017.

[8] R.C. Wiens, S. Maurice, B. Barraclough, M. Saccoccio, W.C. Barkley, J.F. Bell, S. Bender, J. Bernardin, D. Blaney, J. Blank, M. Bouye, N. Bridges, N. Bultman, P. Cais, R.C. Clanton, B. Clark, S. Clegg, A. Cousin, D. Cremers, A. Cros, L. Deflores, D. Delapp, R. Dingler, C. D'Uston, M. Darby Dyar, T. Elliott, D. Enemark, C. Fabre, M. Flores, O. Forni, O. Gasnault, T. Hale, C. Hays, K. Herkenhoff, E. Kan, L. Kirkland, D. Kouach, D. Landis, Y. Langevin, N. Lanza, F. Larocca, J. Lasue, J. Latino, D. Limonadi, C. Lindensmith, C. Little, N. Mangold, G. Manhes, P. Mauchien, C. McKay, E. Miller, J. Mooney, R. V. Morris, L. Morrison, T. Nelson, H. Newsom, A. Ollila, M. Ott, L. Pares, R. Perez, F. Poitrasson, C. Provost, J.W. Reiter, T. Roberts, F. Romero, V. Sautter, S. Salazar, J.J. Simmonds, R. Stiglich, S. Storms, N. Striebig, J.J. Thocaven, T. Trujillo, M. Ulibarri, D. Vaniman, N. Warner, R. Waterbury, R. Whitaker, J. Witt, B. Wong-Swanson, The ChemCam instrument suite on the Mars Science Laboratory (MSL) rover: Body unit and combined system tests, Space Sci. Rev. 170 (2012) 167–227. doi:10.1007/s11214-012-9902-4.

[9] T. Ishizuka, Laser Emission Spectrography of Rare Earth Elements, 504 (1967) 8–11.

[10] S.S. Harilal, P. Radhakrishnan, V.P.N. Nampoori, C.P.G. Vallabhan, Temporal and spatial evolution of laser ablated plasma from $YBa_2Cu_3O_7$, Appl. Phys. Lett. 64 (1994) 3377–3379. doi:10.1063/1.111280.

[11] S.G. Buckley, H.A. Johnsen, K.R. Hencken, A.D.W. Hahn, Implementation of laser-induced breakdown spectroscopy as a continuous emissions monitor for toxic metals, Waste Manag. 20 (2000) 455–462. doi:10.1016/S0956-053X(00)00011-8.

[12] P. Fichet, M. Tabarant, B. Salle, C. Gautier, Comparisons between LIBS and ICP/OES, Anal. Bioanal. Chem. 385 (2006) 338–344. doi:10.1007/s00216-006-0384-7.

[13] M. Martin, R.C. Martin, S. Allman, D. Brice, A. Wymore, N. Andre, Quantification of rare earth elements using laser-induced breakdown spectroscopy, Spectrochim. Acta - Part B At. Spectrosc. 114 (2015) 65–73. doi:10.1016/j.sab.2015.10.005.

[14] T.A. Labutin, S.M. Zaytsev, A.M. Popov, N.B. Zorov, A novel approach to sensitivity evaluation of laser-induced breakdown spectroscopy for rare earth elements determination, J. Anal. At. Spectrom. 31 (2016) 2223–2226. doi:10.1039/C6JA00200E.

[15] M. Saxon, M. Leijd, K. Forrester, J. Berg, Geology, mineralogy, and metallurgical processing of the Norra Kärr heavy REE deposit, Sweden, Symp. Strateg. Crit. Mater. Proceedings, Novemb. 13-14, 2015. (2015) 97–107.

[16] A.S.L. Sjöqvist, D.H. Cornell, T. Andersen, M. Erambert, M. Ek, M. Leijd, Three Compositional Varieties of Rare-Earth Element Ore: Eudialyte-Group Minerals from the Norra Kärr Alkaline Complex, Southern Sweden, Minerals. 3 (2013) 94–120. doi:10.3390/min3010094.

[17] B. Castor, J.B. Hedrick, Rare Earth Elements, in: S.T. Kogel, Jessica Elzea; Trivedi, Nikhil C.; Barker, James M.; Krukowski (Ed.), Ind. Miner. Rocks, Society for Mining, Metallurgy and Exploration, 2006: pp. 769–792. doi:10.1007/978-3-642-35458-8.

[18] I.T. Jolliffe, Principal Component Analysis, Second Edition, Encycl. Stat. Behav. Sci. 30 (2002) 487. doi:10.2307/1270093.

[19] H. Abdi, L.J. Williams, Principal component analysis, Wiley Interdiscip. Rev. Comput. Stat. 2 (2010) 433–459. doi:10.1002/wics.101.

[20] M. Wall, A. Rechtsteiner, L.M. Rocha, Singular value decomposition and principal component analysis, in: D.P. Berrar, W. Dubitzky, M. Granow (Eds.), A Pract. Approach to Microarray Data Anal., Kluwer, 2003: pp. 1–18. doi:10.1007/0-306-47815-3_5.

[21] Matlab Documentation, MathWorks, Inc. (n.d.). https://se.mathworks.com/help/matlab/ref/svd.html (accessed May 5, 2017).

[22] J. Klus, P. Mikysek, D. Prochazka, P. Pořízka, P. Prochazková, J. Novotný, T. Trojek, K. Novotný, M. Slobodník, J. Kaiser, Multivariate approach to the chemical mapping of uranium in sandstone-hosted uranium ores analyzed using double pulse Laser-Induced Breakdown Spectroscopy, Spectrochim. Acta - Part B At. Spectrosc. 123 (2016) 143–149. doi:10.1016/j.sab.2016.08.014.

[23] P. Pořízka, J. Klus, A. Hrdlička, J. Vrábel, P. Škarková, D. Prochazka, J. Novotný, K. Novotný, J. Kaiser, Impact of Laser-Induced Breakdown Spectroscopy data normalization on multivariate classification accuracy, J. Anal. At. Spectrom. (2016) 277–288. doi:10.1039/C6JA00322B.

[24] I.R. Lewis, H. Edwards, Handbook of Raman spectroscopy: From the research Laboratory to the Process Line, CRC Press, 2001.

[25] M.H. Trauth, MATLAB Recipes for Earth Sciences, 2nd edition, Springer-Verlag Berlin Heidelberg, 2007. doi:10.1007/978-3-540-72749-1.

[26] M. Gaft, R. Reisfeld, G. Panczer, Modern Luminescence Spectroscopy of Minerals and Materials, 1st ed., Springer-Verlag Berlin Heidelberg, 2005.

[27] J. Kramida, A., Ralchenko, Yu., Reader, NIST Atomic Spectra Database (ver. 5.3), [Online], Natl. Inst. Stand. Technol. Gaithersburg, MD. (2015).

[28] O.J. Adamson, The Petrology of the Norra Kärr District. An occurrence of alkaline Rocks in Southern Sweden, Geol. Föreningen I Stock. Förhandlingar. 66 (1944) 112–255.

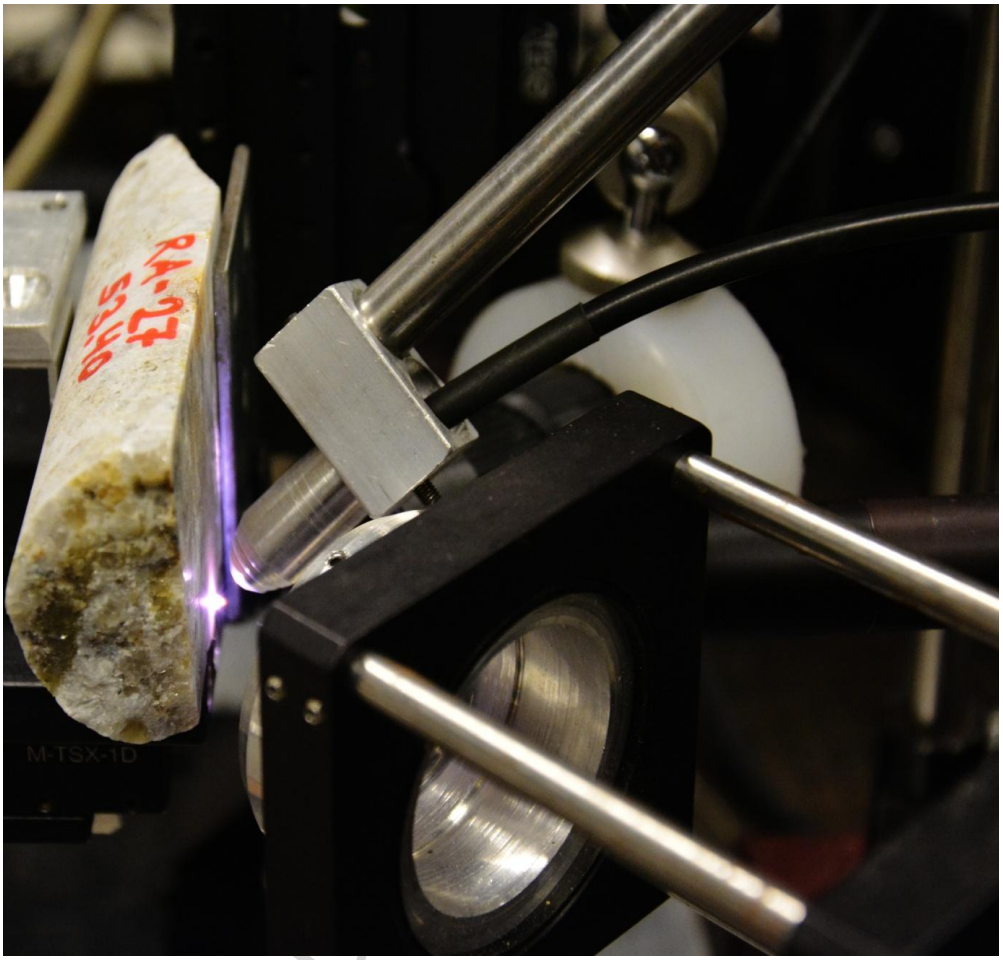


Graphical abstract

**Highlights**

Yttrium occurrence has been located in rock samples using laser-induced breakdown spectroscopy

Mineral classification based on singular value decomposition for rare earth element ores is presented

Mineralogical map of drill core samples has been constructed